

The interaction operator from PEC to ES can be derived from Eq. (20) by setting $M_1 = 0$. Moreover, the interaction operator from ES to PEC is

$$\begin{bmatrix} \mathbf{J}_2 \\ \frac{1}{\eta} \mathbf{t}_2 \end{bmatrix} = T^{ph} \cdot \begin{bmatrix} \mathbf{J}_1 \\ \frac{1}{\eta} \mathbf{M}_1 \\ \frac{1}{\eta} \mathbf{t}_1 \end{bmatrix} = \begin{bmatrix} L_{21}^{EJ} & \eta K_{21}^{EM} & 0 \\ 0 & 0 & 1 \end{bmatrix} \cdot \begin{bmatrix} \mathbf{J}_1 \\ \frac{1}{\eta} \mathbf{M}_1 \\ \frac{1}{\eta} \mathbf{t}_1 \end{bmatrix}. \quad (22)$$

Hence, the equation for the example in Figure 2 can be written as the following,

$$\begin{aligned} \begin{bmatrix} L_{11} & L_{13} \\ L_{31} & L_{33} \end{bmatrix} \cdot \begin{bmatrix} \mathbf{J}_1 \\ \mathbf{J}_3 \end{bmatrix} + T_{12}^{PH} \cdot \begin{bmatrix} \mathbf{J}_{eq}^o \\ \frac{1}{\eta} \mathbf{M}_{eq}^o \\ \frac{1}{\eta} \mathbf{t}_2^o \end{bmatrix} = - \begin{bmatrix} L_{10} \\ L_{30} \end{bmatrix} \cdot \begin{bmatrix} \mathbf{J}_0 \end{bmatrix} \\ - S_{22} \cdot T_{21}^{HP} \cdot \begin{bmatrix} \mathbf{J}_1 \\ \frac{1}{\eta} \mathbf{t}_1 \end{bmatrix} + \begin{bmatrix} \mathbf{J}_{eq}^o \\ \frac{1}{\eta} \mathbf{M}_{eq}^o \\ \frac{1}{\eta} \mathbf{t}_2^o \end{bmatrix} = S_{22} \cdot \begin{bmatrix} \mathbf{J}_eq^i \\ \frac{1}{\eta} \mathbf{M}_{eq}^i \\ \frac{1}{\eta} \mathbf{t}_2^i \end{bmatrix}. \quad (23) \end{aligned}$$

4. NUMERICAL EXAMPLES

Here we will show one example of a two-monopole array mounted on a ground plane as shown in Figure 3(a). Two ES's that intercept the ground plane are used to enclose the antennas [Fig. 3(b)]. Triangular mesh and RWG basis [11] are used to discretize the structure. There are 779 unknowns on the whole antenna and 476 unknowns on each ES. The simulation frequency is 0.3 GHz, and the length of the monopole is a quarter wavelength. The excitation is a multiple- δ -gap source added on the left arm. Figure 4 shows the equivalent current distribution, and Figure 5(b) shows the radiation field using the direct method and EPA. The two results agree with each other very well.

5. CONCLUSIONS

The equivalence principle algorithm is introduced in this communication. It is based on MOM and equivalence principle. Tap basis is introduced to model a continuous current intercepting the equivalent surface. Using this scheme, the current continuity is conserved and the singularity of the charges is avoided. Moreover, it is more stable and accurate than using a fictitious junction basis.

REFERENCES

- Y.J. Lu and C.Y. Shen, A domain decomposition finite-difference method for parallel numerical implementation of time-dependent Maxwell's equations, *IEEE Trans Antennas Propag* 45 (1997), 556–562.
- B. Stupfel and M. Mognot, A domain decomposition method for the vector wave equation, *IEEE Trans Antennas Propag* 48 (2000), 653–660.
- M.N. Vouvakis and L. Jin-Fa, A finite element domain decomposition technique for the analysis of large electromagnetic problems, *IEEE Antennas and Propagation Society International Symposium*, 2005, vol. 174B, pp 173–176.
- Y. Chen, A fast, direct algorithm for the Lippmann-Schwinger integral equation in two dimensions, *Adv Comput Math* 16 (2002), 175–190.
- M.K. Li, W.C. Chew, and L.J. Jiang, A domain decomposition scheme based on equivalence theorem, *Microwave Opt Technol Lett*, 48 (2006), 1853–1857.
- W.C. Chew and C.C. Lu, The use of Huygens equivalence principle for solving the volume integral-equation of scattering, *IEEE Trans Antennas Propag* 41 (1993), 897–904.
- M.A. Jensen, Recursive green's function technique for acoustic scattering from heterogeneous objects, *J Acoust S Am* 103 (1998), 713–720.
- C.C. Lu and W.C. Chew, The use of Huygens equivalence principle for solving 3-d volume integral-equation of scattering, *IEEE Trans Antennas Propag* 43 (1995), 500–507.
- A.M. van de Water, B.P. de Hon, M.C. van Beurden, A.G. Tijhuis, and P. de Maagt, Linear embedding via Green's operators: A modeling technique for finite electromagnetic band-gap structures, *Phys Rev E* 72 (2005).
- W.C. Chew, Waves and fields in inhomogeneous media, IEEE Press, New York, 1995.
- S.M. Rao, D.R. Wilton, and A.W. Glisson, Electromagnetic scattering by surfaces of arbitrary shape, *IEEE Trans Antennas Propag* 30 (1982), 409–418.

© 2006 Wiley Periodicals, Inc.

A CONTINUOUSLY STEERABLE ARRAY ANTENNA USING MOVABLE DIELECTRIC SLABS ON A COPLANAR WAVEGUIDE

Junho Cha,¹ Yasuo Kuga,¹ and Sangil Lee²

¹ Department of Electrical Engineering, University of Washington, Box 352500, Seattle, WA 98195

² Electronics Engineering Department, Mokpo National University, Chonman, Korea

Received 20 June 2006

ABSTRACT: A simple steerable array antenna is designed using a movable dielectric phase shifter. The change of the effective dielectric constant at different dielectric slab positions on a coplanar waveguide is used as the phase shifter. The impedance matching and desired phase shift conditions are satisfied at two slab heights, and reflection is designed to be minimized at all slab positions. A four-element steerable array antenna at 5.8 GHz is fabricated and measured for testing purposes. © 2006 Wiley Periodicals, Inc.

Microwave Opt Technol Lett 48: 2222–2227, 2006; Published online in Wiley InterScience (www.interscience.wiley.com). DOI 10.1002/mop.21920

Keywords: steerable array antenna; phase shifter

1. INTRODUCTION

In this paper, we introduce a movable dielectric slab placed close to a coplanar waveguide (CPW) which can be used as a phase shifter for the array antenna. The proposed array antenna consists of a patch array antenna, phase shifter, and feed network with a preset delay line as shown in Figure 1. It is noted that the most significant and difficult part of the simulation and fabrication process is the design of the phase shifter [1]. In order to obtain the optimum combinations of a transmission line (TL) structure and material, several TL structures have been investigated. These include a microstrip TL, a coplanar TL without gaps, and a coplanar TL with gaps. Our study shows that the microstrip TL and coplanar TL without gaps are insensitive to the position of a dielectric slab and are eliminated from consideration. In addition, it is found that a high- ϵ_r material such as BaTiO₃ is not suited for a phase shifter. It appears that the electromagnetic field perturbation caused by a high- ϵ_r material is significant, and the proposed design does not work as a phase shifter. The effective dielectric constant and the characteristic impedance are calculated as a function of slab

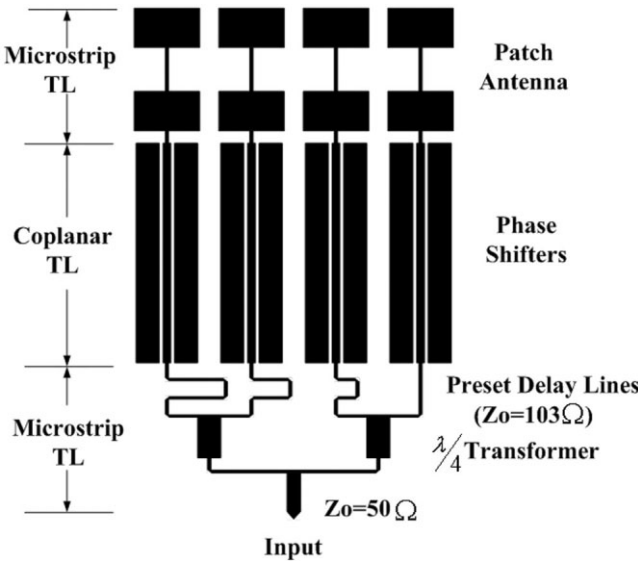


Figure 1 Block diagram of a 4-element steerable array antenna

height. We compare the simulated radiation patterns and the measured radiation patterns of the steerable array antenna at 5.8 GHz.

2. CONTINUOUS PHASE SHIFTER BASED ON A MOBILE DIELECTRIC SLAB

The basic concept of the phase shifter is illustrated in Figure 1. The CPW has air gaps between the center signal line and ground lines. As the movable dielectric slab moves closer or into the gap of the CPW, the effective dielectric constant changes and it is given as a function of d for a given structure. In this paper, we assume that the slab can be moved continuously from the flash on the substrate ($d = 0$ or very small) to far away from the substrate ($d = \infty$ or $d > 2$ mm in our case).

The width of the signal trace is S and the width of the ground trace is G_w . The gap between the ground and the signal is G . Substrate thickness is h and the height of the dielectric material is 5 mm. The length of the dielectric material is l .

This structure can be modeled as an unmatched TL section (or a layered structure). The transmission coefficient T of a layered structure is given as [2]

$$T = \frac{(1 - \Gamma_1^2) e^{-j\theta}}{1 - \Gamma_1^2 e^{-2j\theta}}, \quad (1)$$

where Γ_1 is the reflection coefficient at the boundary due to a semi-infinite layer and θ is the phase shift due to a slab. When θ becomes an integer multiple of $1/2$, it is well known that the reflection from the slab diminishes (or T becomes 1). This is the impedance matching condition. In addition, the phase shift of the slab section when d is changed from $d = \infty$ to $d = 0$ will be related to the effective dielectric constant of these two states [3]. Our primary concern will be a good impedance matching at all values of d . First, we set the matched impedance condition at $d = 0$ and $d = \infty$. Since the integer multiple of the $\lambda/2$ condition must be satisfied at $d = 0$, this will determine the available length of each slab. At $d = \infty$ or without slab, the impedance is always matched. The main task, therefore, is to estimate the effective dielectric constant of CPW with a slab on it. This process requires knowledge of the material characteristics, TL structure, and a good 3-D simulation tool. Because we are designing a low-cost antenna, we

use a CPW structure fabricated on an FR-4 type substrate (IS620 from Iola) which has a thickness of 1.6 mm and $\epsilon_{\text{sub},d} = 3.73$. The CPW has a signal trace width of 2 mm and a ground trace width of 6 mm. The gap between the ground and the signal is 1 mm. Without the dielectric slab ($d = 5$ mm or effectively $d = \infty$), the CPW has a characteristic impedance of $Z_0 = 103 \Omega$ and an effective dielectric constant of $\epsilon_{\text{effective}} = 1.4$. To simplify the fabrication process, we also used dielectric slabs without protruding notches in the initial design. Therefore, when $d = 0$, the CPW gap is filled with air rather than with the dielectric material. The dielectric constant of the slab must be much higher than that of the substrate, but it cannot be too high. It is found that a high- ϵ_r material such as BaTiO₃ creates a strong electromagnetic field perturbation and is not useful as a slab in our design. We chose the Teflon-ceramic composite with $\epsilon_r = 10.5$ as a slab. Using HFSS simulations, the desired effective dielectric constant is found to be about $\epsilon_{\text{effective}} = 7.76$ when $d = 0$. This will determine the length of the $\lambda/2$ section to be 9.32 mm, and the amount of phase shift with respect to the $d = \infty$ condition is 105°. Therefore, if we want to introduce a 105° phase difference among four antenna elements, the length should be 0, $\lambda/2$, λ , and $3\lambda/2$. Since we cannot find an analytical formula to estimate $\epsilon_{\text{effective}}$ for $d > 0$, extensive HFSS simulations are conducted for $0 < d < 5$ mm. Because the slab length is set close to the integer multiple of $\lambda/2$ when $d = 0$, the reflection from this slab will be small at $d = 0$. By setting, we can approximate T in Eq. (1) as $T \approx e^{-j\theta}$. Then the phase change at the slab height d with respect to that without a dielectric slab ($d = \infty$) can approximately be expressed as

$$\theta_d \approx k_0 L_d \left(\sqrt{\epsilon_{\text{eff},d}} - \sqrt{\epsilon_{\text{eff},d=\infty}} \right), \quad (2)$$

where k_0 is the wavenumber in free space and L_d is the slab length. $\epsilon_{\text{eff},d=\infty}$ represents the effective dielectric constant when the dielectric material is far enough away from the substrate, and $\epsilon_{\text{eff},d}$ represents the effective dielectric constant when the slab height is d . The effective dielectric constant for $0 < d < 5$ mm is estimated from this phase. Table 1 presents numerical results for the G-S-G CPW with the center gap for cases with and without the dielectric material. The characteristic impedance and the effective dielectric constant change depending on the distance of the dielectric material from the substrate. As expected, the impedance is matched at $d = 5$ and 0. When $d = 1.25$ mm, there is a slight impedance mismatch, although S_{21} is still close to 1. Figure 2 shows the effective dielectric constant as a function of distance d . Beyond $d > 2$ mm, the slab is completely out of the CPW and there is no change in $\epsilon_{\text{effective}}$. The effective dielectric constant gradually changes from $d = 2$ mm to $d = 0.25$ mm and then increases rapidly at $d = 0$. We chose the phase difference of -105° to $+105^\circ$ between adjacent elements, because the phase difference between $d = 5$ mm and $d = 0$ is 105° in Table 1.

TABLE 1 Simulated Results at $d = 5$ mm, $d = 1.25$ mm, and $d = 0$

Parameter	d (mm)		
	5	1.25	0
$ S_{21} $	0.99	0.91	0.98
$ S_{11} $	0.01	0.36	0.02
Characteristic impedance (Ω)	103	83	51
Effective dielectric constant	1.4	3.73	7.76
Phase difference based on $d = 5$ mm	0°	49.5°	105°

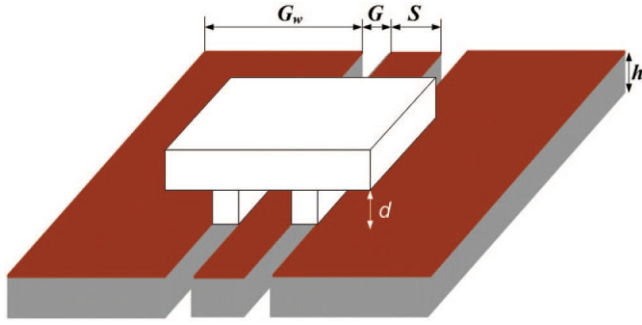


Figure 2 Effective dielectric constant vs. height d from the substrate. [Color figure can be viewed in the online issue, which is available at www.interscience.wiley.com]

Figure 3 shows the magnitudes of S_{21} and S_{11} as a function of d . As expected, good matching (small S_{11}) can be obtained at $d = 0$ and $d > 2$ mm, but the maximum value can reach to 0.366 at $d = 1.25$ mm. The transmission coefficient, however, is always greater than 0.9 at all positions of d . Although we cannot satisfy the impedance matching condition at all values of d for the continuous phase shifter, S_{11} is still less than -9 dB (0.366) for this phase shifter.

3. DESIGN OF THE FEED NETWORK USING THE PRESET DELAY LINES

In order to reduce the number of phase shifters to $N-1$ where N is the number of arrays, the preset delay line is added to each feed line as shown in Figure 1. The basic concept is illustrated in Figure 4. Suppose the antenna is designed with a phase difference of -105° to $+105^\circ$ between adjacent elements, then the required phases at different antenna elements are shown in Figure 4. The Antenna Element 1 which is shown as S_{21} does not require an adjustable phase shifter, but it must have a -105° preset phase with respect to Element 2 (S_{31} in Fig. 4). The largest phase shift of 630° is required for Element 4 (S_{51} in Fig. 4). Therefore, by introducing the preset delay line, we can eliminate one phase shifter.

The CPW has the characteristic impedance of $Z_0 = 103 \Omega$ with $d = 5$ mm and an input impedance of the patch antenna of 103Ω .

Effective dielectric constant ($\epsilon_{\text{effective}}$) as a function of slab height

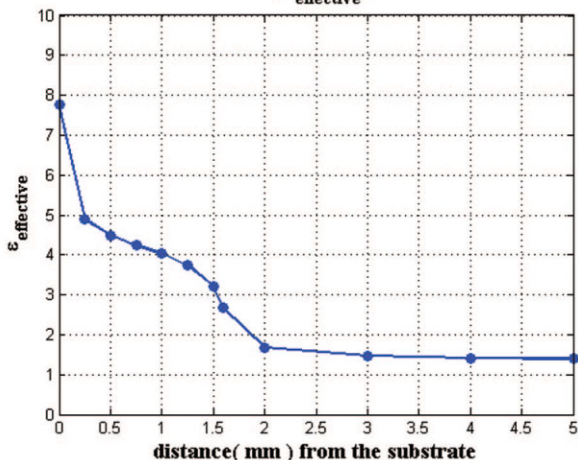


Figure 3 Simulated S_{21} and S_{11} results from $d = 0$ to $d = 5$ mm. [Color figure can be viewed in the online issue, which is available at www.interscience.wiley.com]

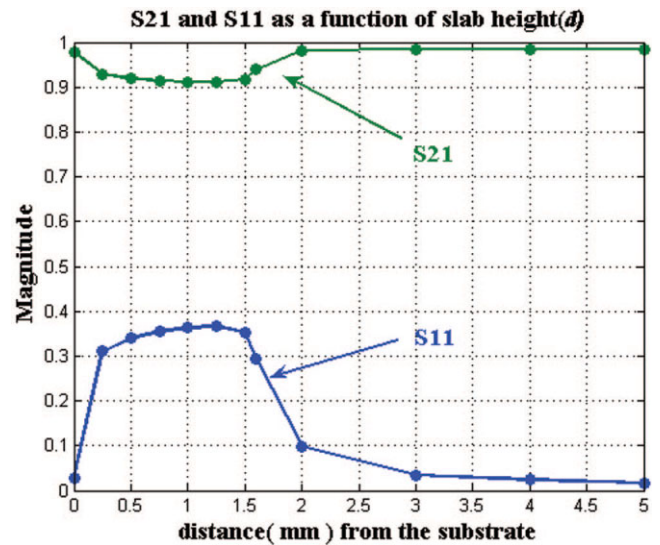


Figure 4 Phase difference among four elements from -105° to $+105^\circ$

The main problem with the proposed phase shifter is that the characteristic impedance also changes when the dielectric slab position is changed from $d = 5$ mm ($Z_0 = 103 \Omega$) to $d = 0$ ($Z_0 = 51 \Omega$). The lowest Z_0 occurs at $d = 0$, and thus the circuit must be designed to minimize the reflection at $d = 0$. In order to reduce the unwanted reflection, the effective length of the CPW is set with $d = 0$ to be $m\lambda/2$ where m is an integer. Because a $\lambda/2$ section does not create a reflection, this will guarantee the impedance matching at $d = 0$. At other slab positions, we estimate the characteristic impedance using HFSS. Table 2 shows the required slab height d and the characteristic impedance Z_0 for the 4-element array antenna with the phase difference at -105° , 0° , and $+105^\circ$. Although the reflection is minimized at $d = 0$ and $d = 5$ mm, we have an impedance mismatch at $d = 0.5$ mm as shown in Table 2. For the element phase differences of -105° to $+105^\circ$, we can obtain the antenna beam scan angle of -40° to $+40^\circ$.

4. FABRICATION OF A 4-ELEMENT STEERABLE ARRAY ANTENNA AT 5.8 GHZ

To demonstrate the feasibility of our concept, a 4-element steerable array antenna is designed and fabricated at 5.8 GHz for a wireless network. The array antenna is designed to scan with a phase difference of -105° to $+105^\circ$ and with an expected beam scan angle of -40° to $+40^\circ$.

Figure 5 shows the fabricated 4×1 and 4×2 array antenna with and without the dielectric slabs [4, 5]. The substrate is IS620 with $\epsilon_{\text{sub}} = 3.73$ and a thickness of 1.6 mm. The height of the dielectric slab is 5 mm with a dielectric constant of $\epsilon_r = 10.5$, which was obtained using Duroid 6010. The width of the patch antenna is 17 mm and the height of the patch antenna is 12.66 mm. In order to remove the grating mode, the antenna separation is set to 22 mm, which is less than $\lambda/2$ while the input impedance is 103

TABLE 2 Phase Relationship of 4-Element Array at 3 Phase (Slab Positions: -105° , 0° , and $+105^\circ$)

Phase	Distance (mm)	Distance				
		S_{21}	S_{31}	S_{41}	S_{51}	Z_0
-105°	$d=0$	0°	210°	420°	630°	51
0°	$d=0.5$	0°	105°	210°	315°	77
$+105^\circ$	$d=5$	0°	0°	0°	0°	103

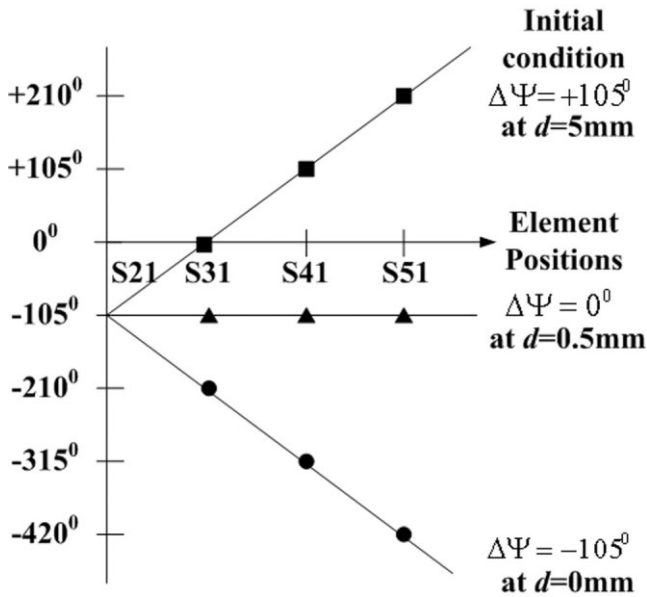


Figure 5 Photographs of a 4×1 and 4×2 array antenna with and without dielectric slabs. [Color figure can be viewed in the online issue, which is available at www.interscience.wiley.com]

Ω . The preset delay lines in Figure 6 have -315° for Element 1, -210° for Element 2, and -105° , for Element 3, whereas the dielectric slabs introduce a maximum phase shift of -210° for Element 2, -420° for Element 3, and -630° for Element 4. This corresponds to the phase diagram shown in Figure 4. The lengths of the dielectric slabs on the CPW are 20.9, 41.8, and 62.7 mm.

Figure 6 shows the simulated H-plane radiation patterns of a 4×1 array antenna at 5.8 GHz. Figure 6(a) is for $d = 0$ with the peak at 30° , (b) is for $d = 0.1$ mm with the peak close to 0° , and (c) is for $d = 5$ mm with the peak at -40° . Figure 7 shows the measured H-plane radiation pattern of a 4×1 array antenna for the same three values of d . We obtain good agreement for the $d = 0$ and $d = 0.1$ mm cases, but when the slab is on the CPW, the peak of the beam is only at 13° . This discrepancy seems to be due to a small residual gap ($<10 \mu\text{m}$) between the dielectric slab and conductors, and it is difficult to avoid when using the flat bottom slabs. In order to solve this problem, we added protruding notches

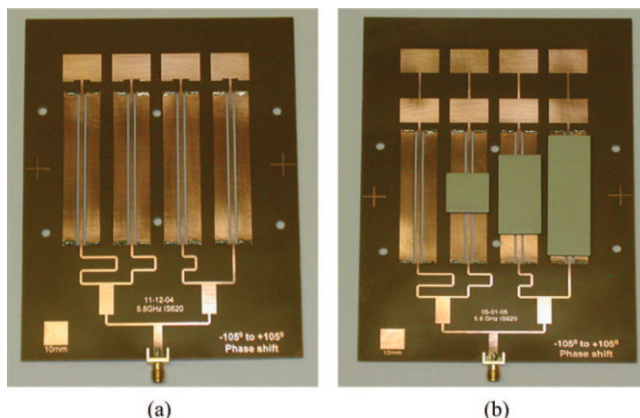


Figure 6 Simulated H-plane radiation patterns of a 4×1 array antenna at 5.8 GHz. (a) $d = 0$ mm, (b) $d = 0.1$ mm, and (c) $d = 5$ mm. [Color figure can be viewed in the online issue, which is available at www.interscience.wiley.com]

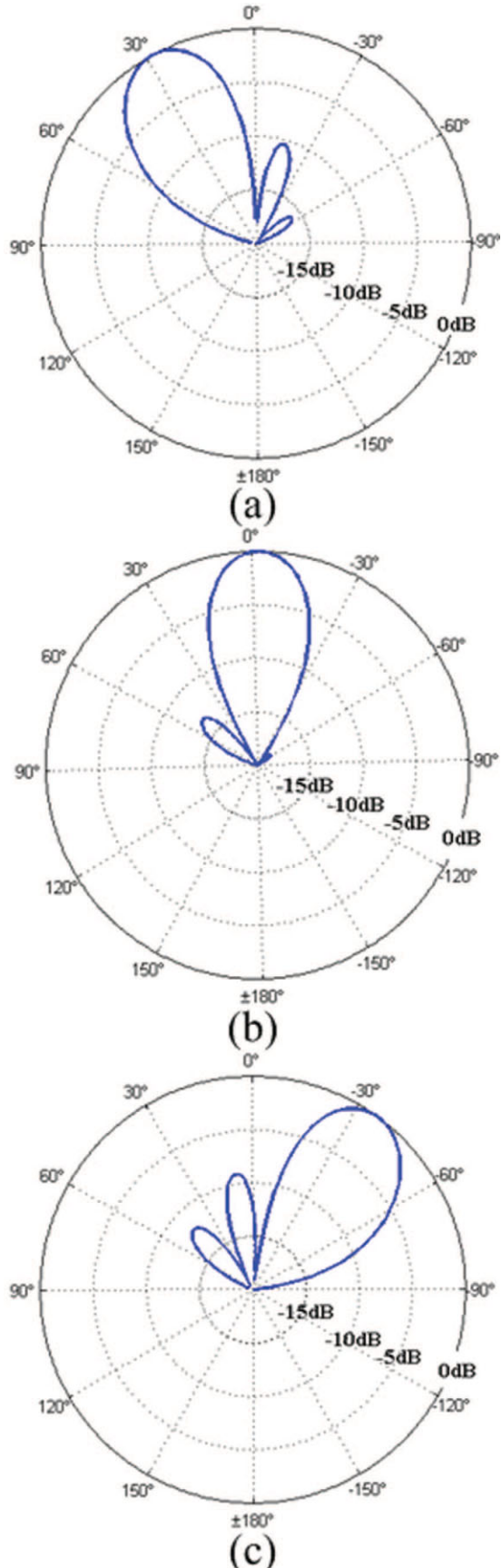


Figure 7 Measured H-plane radiation patterns of a 4×1 array antenna at 5.8 GHz. (a) $d = 0$, (b) $d = 0.1$ mm, and (c) $d = 5$ mm. [Color figure can be viewed in the online issue, which is available at www.interscience.wiley.com]

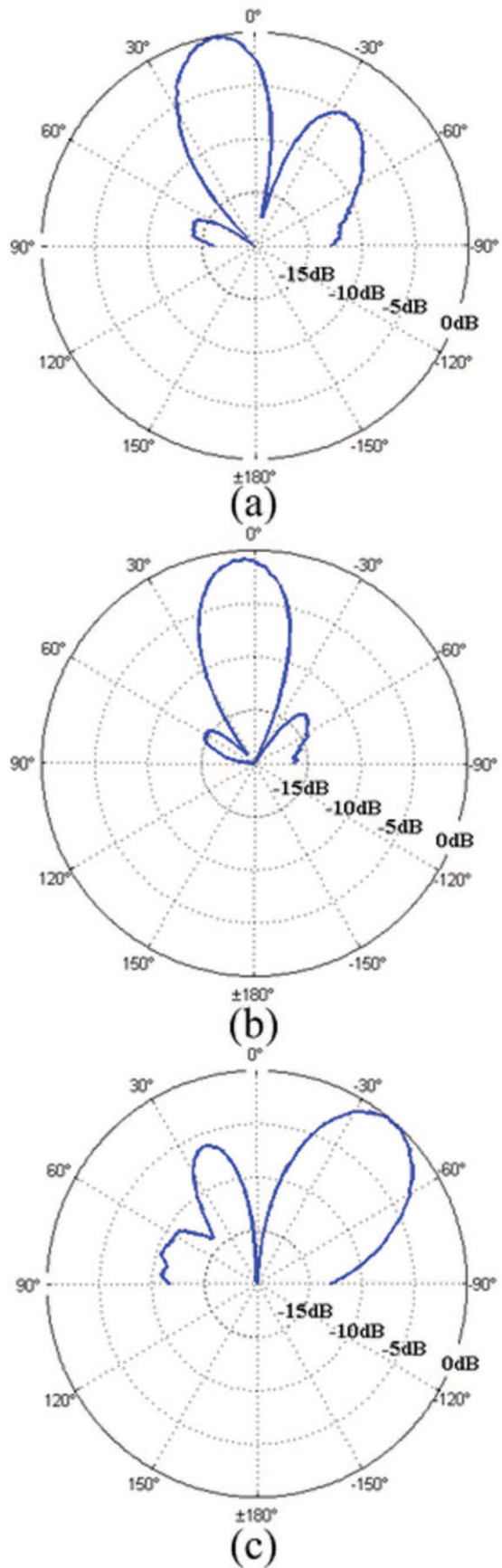


Figure 8 Phase shifter. A 3-D schematic of a ground-signal-ground (G-S-G) CPW with a movable dielectric slab. [Color figure can be viewed in the online issue, which is available at www.interscience.wiley.com]

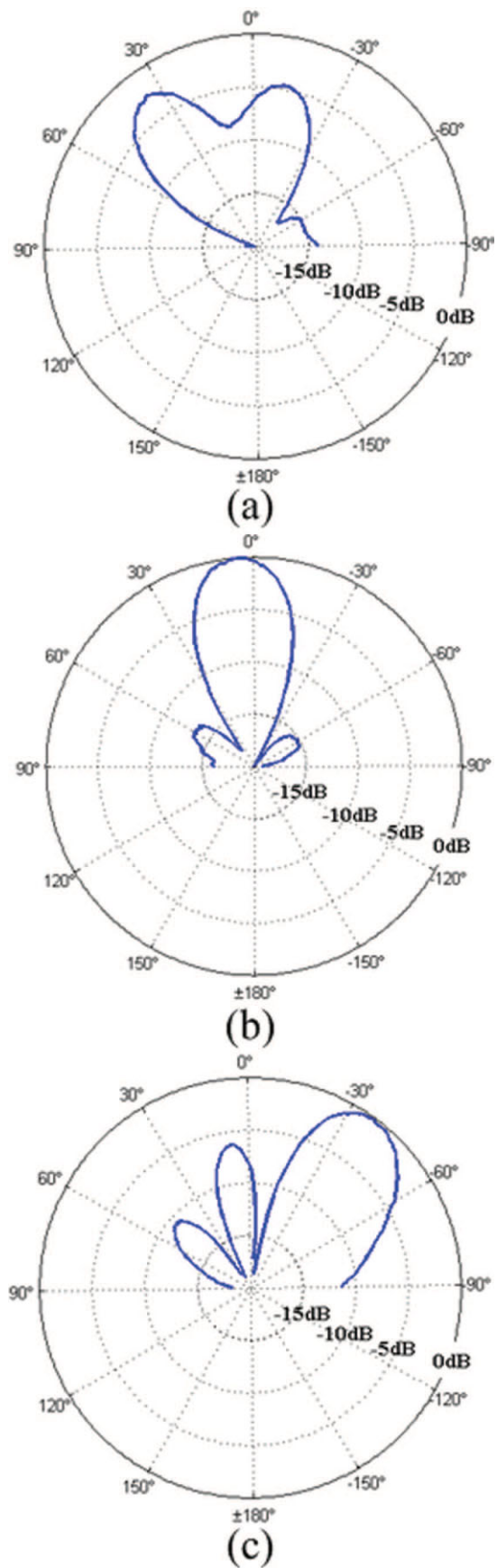


Figure 9 Measured H-plane radiation patterns of a 4×2 array antenna at 5.8 GHz. (a) $d = 0\text{ mm}$ with small notches, (b) $d = 0.1\text{ mm}$, and (c) $d = 5\text{ mm}$. [Color figure can be viewed in the online issue, which is available at www.interscience.wiley.com]

to the flat bottom dielectric slabs, and tested them with a 4×2 array antenna. This modification makes the shape of slabs similar to the one shown in Figure 8. Figure 9 shows the H-plane radiation patterns of three cases. With the addition of small notches, the antenna beam can now be scanned up to $+40^\circ$.

5. CONCLUSIONS

A novel design of a steerable array antenna has been demonstrated. The phase shifter is based on a movable dielectric slab placed close to a CPW with air gaps. The impedance mismatch can be avoided by choosing the slab dielectric constant and length for the two extreme positions, namely at $d = 0$ and $d \approx 2$ mm. It may be possible to further reduce S_{11} by optimizing the impedance mismatching position at $d > 0$ instead of $d = 0$. We also show that the use of preset delay lines can reduce the number of phase shifters. Although the test antenna is designed for 5.8 GHz, the technique can be applied at a much higher frequency. One possible application is for the 77 GHz automobile collision avoidance radar [6].

ACKNOWLEDGMENTS

This project was supported by National Science Foundation ECS-0424414. The authors thank J. Kajiya and J. Ritcey for useful discussions and suggestions.

REFERENCES

- Y. Kuga, J. Cha, J.A. Ritcey, and T. Kajiya, Mechanically steerable antennas using dielectric phase shifters, IEEE AP-S International Symposium, Monterey, CA, 2004, pp. 161–164.
- J. Baker-Jarvis and E.J. Vanzura, Improved technique for determining complex, permittivity with the transmission/reflection method, IEEE Trans Microwave Theory Tech 38 (1990), 1096–1101.
- J. Cha, Y. Kuga, and T. Kajiya, Mechanically steerable antennas with controllable, microwave phase shifters at 20 GHz, IEEE AP-S International Symposium, Washington D.C., 2005, pp. 691–694.
- C.F. Wang, F. Ling, and J.M. Jin, A fast full-wave analysis of scattering and radiation from large finite arrays of microstrip antennas, IEEE Trans Antennas Propagat AP-46 (1998), 1467–1474.
- K.L. Wu, M. Spenuk, J. Litva, and D.G. Fang, Theoretical and experimental study of feed network effects on the radiation pattern of series-fed microstrip antenna arrays, IEE Proceedings-H 138 (1991), No. 3.
- J. Cha and Y. Kuga, A mechanically steerable array antenna using controllable dielectric phase shifters for 77 GHz automotive radar systems, IEEE AP-S International Symposium, Albuquerque, NM, 2006.

© 2006 Wiley Periodicals, Inc.

GROWTH AND STUDIES OF OPTICAL PROPERTIES OF DOUBLE-DOPED In:Fe:LiTaO₃ CRYSTAL

Decai Ma,¹ Biao Wang,^{1,2,3} Shuangquan Fang,¹ Tao Zhang,¹ Rui Wang,¹ and Yuan Wei¹

¹ School of Astronautics
Harbin Institute of Technology
Harbin 150001, China

² State Key Laboratory of Optoelectronic Materials and Technologies
Institute of Optoelectronic and Functional Composite Materials
Sun Yat-Sen University
Guangzhou 510275, China

³ School of Physics Science and Engineering
Sun Yat-Sen University
Guangzhou 510275, China

Received 16 April 2006

ABSTRACT: *In:Fe:LiTaO₃* crystals were grown in an air atmosphere using the Czochralski method. The photorefractive properties were measured by the two-wave coupling experiments, and light-induced scattering was used to characterize the optical damage. It was found that the photorefractive response speed of *In:Fe:LiTaO₃* was about four times faster than that of *Fe:LiTaO₃*, and the resistance ability to optical damage was drastically improved. The increase in damage resistance and faster response speed could be attributed to the Fe³⁺ losing their electron acceptor properties and, therefore, an increase in photoconductivity. © 2006 Wiley Periodicals, Inc. *Microwave Opt Technol Lett* 48: 2227–2230, 2006; Published online in Wiley InterScience (www.interscience.wiley.com). DOI 10.1002/mop.21919

Key words: *In:Fe:LiTaO₃* crystal; exponential gain coefficient; diffraction efficiency; response speed; photodamage resistance

1. INTRODUCTION

Doped lithium tantalum (LiTaO₃, LT) crystals exhibit excellent photorefractive properties, and this attractive feature makes them important for applications in piezoelectric, electro-optic, surface acoustic wave, waveguide, and nonlinear optical devices [1–5]. Doping with transition metal or rare earth ions into crystals can affect efficiency, sensitivity, speed, and spectral response of photorefractive effect. A great amount of studies on LiTaO₃ included crystals containing various dopants, such as Fe, Ce [6], Zn [7], Cr [8], Tm [9], Ho [10], and so on. Fe:LiTaO₃ crystal has been selected as one of holographic storage media for industrial use. In Fe:LiTaO₃ crystal, Fe²⁺ ions acted as electron donors, and Fe³⁺ ions act as electron traps. Electrons are excited from Fe²⁺ to the conduct band, and then are redistributed because of diffusion, drift, and bulk photovoltaic effect. Finally, Fe³⁺ will capture the electrons and a space charge field builds up. The refractive index can be modulated by electro-optic effect. Fe:LiTaO₃ crystal has the promising application in the volume holographic storage, but there are some disadvantages, e.g. long response time and low photodamage resistance ability. For improving photodamage resistance ability of Fe:LiTaO₃ crystal, in this work, In₂O₃ was doped into Fe:LiTaO₃ crystal. In:Fe:LiTaO₃ crystals grown by Czochralski (CZ) method show excellent photodamage resistance ability. In addition, the response time of the In:Fe:LiTaO₃ crystal decreased to an acceptable degree in comparison with Fe:LiTaO₃ crystal.

2. CRYSTAL GROWTH AND SPECIMEN PREPARATION

All crystals including Fe:LiTaO₃, In:Fe:LiTaO₃, Fe:LiNbO₃, and In:Fe:LiNbO₃, are grown from congruent melts by the conventional CZ method, using an intermediate frequency(IF) furnace. The starting materials used to grow the crystals were Fe₂O₃, In₂O₃,